JACS
JOURNAL OF THE AMERICAN CHEMICAL SOCIETY
Article
pubs.acs.org/JACS

Comparison of the Behavior of Metal−Organic Frameworks and Zeolites for Hydrocarbon Separations

David Peralta,[†,‡] Gérald Chaplais,[†] Angélique Simon-Masseron,[†] Karin Barthelet,[‡] Céline Chizallet,[‡] Anne-Agathe Quoineaud,[‡] and Gerhard D. Pirngruber*[,‡]

[†]Equipe Matériaux à Porosité Controlée (MPC), Institut de Science des Matériaux de Mulhouse (IS2M), LRC CNRS-UHA 7228, ENSCMu, 3 rue Alfred Werner, 68093 Mulhouse Cedex, France

[‡]IFP Énergies Nouvelles, Site of Lyon, BP3, Rond Point échangeur de Solaize, 69360 Solaize, France

Supporting Information

ABSTRACT: The objective of this work was to study the adsorption and separation of the most important families of hydrocarbon compounds on metal−organic frameworks (MOFs), in comparison with zeolites. For this purpose, we have selected four probe molecules, each of them representing one of these families, i.e., *o*- and *p*-xylene as aromatics, 1-octene as an alkene, and *n*-octane as an alkane. The separation of these four molecules was studied by binary breakthrough experiments. To represent the large diversity of MOF structures, the experiments were carried out with (i) two MOFs with coordinatively unsaturated metal sites (CUS), i.e., Cu-btc (HKUST-1) and CPO-27-Ni, (ii) a MOF with an anionic framework and extraframework cations, i.e. RHO-ZMOF, and (iii) two rather apolar zeolitic imidazolate framework (ZIF) materials with different pore sizes, i.e. ZIF-8 and ZIF-76. Zeolite NaY and zeolite *β* were used as polar and apolar reference adsorbents, respectively. The results can be briefly summarized as follows: ZIFs (not carrying any polar functional groups) behave like apolar adsorbents and exhibit very interesting and unexpected molecular sieving properties. CUS-MOFs behave like polar adsorbents but show the specificity of preferring alkenes over aromatics. This feature is rationalized thanks to DFT+D calculations. MOFs with extraframework cations behave like polar (cationic) zeolites.

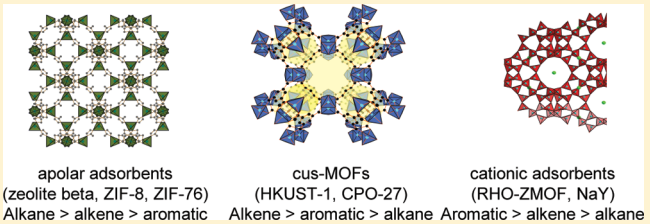

INTRODUCTION

Over several years metal−organic framework (MOF) materials have been intensively investigated in the adsorption and separations of paraffins,[1−6] of aromatic compounds,[7−19] of paraffins from olefins,[20−24] of heteroaromatics,[25−27] and of miscellaneous organic compounds.[13,28] In some of these studies, MOFs were reported to have very peculiar adsorption properties. For example, a non-CUS (coordinatively unsaturated metal sites) copper MOF with oval cages has the unique property of excluding alkanes with more than four carbon atoms in the chain.[1] No other material has yet shown such a neat molecular sieving as a function of chain length. The sieving effect is based on a perfect fit between the cage size of the MOF and the size of *n*-butane. We presume that more examples of such a highly specific shape-selectivity will be discovered because the immense structural diversity of MOFs has allowed one to generate pores with unprecedented shapes and sizes. A second specificity of MOFs is that several structures are highly flexible, as compared to the relatively rigid zeolites. MIL-53-type hybrids are the best known examples of breathing solids that undergo a structural transformation upon adsorption.[29] The breathing may lead to an abrupt change of the selectivity during the course of the separation.[30] Structural flexibility also plays a key role in the adsorption on ZIFs (zeolitic imidazolate frameworks). ZIFs display some of the topologies also encountered in zeolites. The Si−O−Si bonds in zeolites are replaced by M−Im−M bonds (M being a metal cation, usually Zn^{2+} or Co^{2+}, and Im an imidazolate ligand). The positions of the metal centers in ZIF structures are quite rigid, but the imidazolate ligands can rotate (flip) around the M−M axis, thereby modifying the size of the pore aperture.[31,32] This flexibility of the ligands has led to gate opening effects in the adsorption of light hydrocarbons.[24] Another class of MOFs is characterized by the presence of coordinatively unsaturated metal sites (CUS). Such sites act as strong Lewis acids and are usually the preferred adsorption sites for adsorbates. It has been shown that the CUS play a strong role in determining the separation selectivity.[12,13] Finally, it was shown that molecular packing effects may have a strong influence on adsorption in MOFs when the pores are entirely filled with adsorbates. For example, MIL-47, which is an isomorph of MIL-53, is para-selective in the adsorption of a mixture of *p*- and *m*-xylene isomers because two *p*-xylene molecules can stack perfectly on top of each other in the rhombic channel of MIL-47, while the other isomers have to tilt slightly with respect to each other, which weakens the intermolecular interactions.[7] Such packing effects are also frequently encountered in zeolites, for example in silicalite-1,[33−35] ferrierite,[36] and faujasites.[37,38]

Received: December 20, 2011
Published: March 7, 2012

   dx.doi.org/10.1021/ja211864w | *J. Am. Chem. Soc.* 2012, 134, 8115−8126

While the numerous examples cited above point out the specificities of each structure, it remains difficult to catch a general picture of hydrocarbon adsorption on MOFs. Simple rules of thumb and guidelines of how to predict the separation properties of MOFs based on their surface chemistry, pore size, and shape are missing. The aim of the present contribution therefore is to identify some global trends in the adsorption of hydrocarbons on MOFs. In order to cover the large structural diversity of MOFs, we have chosen for this purpose (i) two MOFs with coordinatively unsaturated metal sites, i.e., Cu-btc (HKUST-1) and CPO-27-Ni; (ii) a MOF with an anionic framework and extraframework cations, i.e., RHO-ZMOF; and (iii) two rather apolar ZIF materials with different pore sizes, i.e., ZIF-8 and ZIF-76. The MOFs were compared with a highly polar zeolite containing extraframework cations, i.e., zeolite NaY, and an apolar, purely siliceous zeolite β. The structures of the adsorbents are depicted in the Supporting Information.

For testing the adsorption properties of the selected materials, we have chosen as adsorbates representative molecules of the most important families of hydrocarbons, i.e., alkanes, alkenes, and aromatics. For practical reasons (volatility, toxicity), the C8 compounds octane (*n*C8), 1-octene (=C8), and *p*-xylene (PX) were selected. In order to evaluate the impact of steric effects and polarity within a class of hydrocarbons, *o*-xylene (OX) was further added to the list. The main properties of the probe molecules are summarized in Table 1.

Table 1. Properties of the Probe Molecules[39−41]

	octane	1-octene	*p*-xylene	*o*-xylene
boiling point (K)	399	394	411	417
MIN-1 dimension (Å)	4.0	4.0	4.2	4.2
MIN-2 dimension (Å)	4.5	4.9	6.7	7.5
dipole moment (D)	0.00	0.34	0.00	0.62

The competitive adsorption of these molecules was studied by breakthrough experiments of binary mixtures in the gas phase. Additional FTIR experiments and DFT calculations were employed to rationalize some unexpected trends in the adsorption behavior.

EXPERIMENTAL AND CALCULATION METHODS

Syntheses of Materials. HKUST-1 and CPO-27-Ni were synthesized by scaling up the synthesis protocols described by Bordiga et al. and Dietzel et al. for a 1 L autoclave.[42,43] ZIF-76 was synthesized using the synthesis protocol described in our previous work.[44] ZIF-8 and NaY were purchased from Aldrich (Basolite Z1200) and Zeolyst International, respectively. The siliceous zeolite β was prepared according to the literature.[45]

Due to the lack of reproducibility and the low yield of the RHO-ZMOF synthesis described by the Eddaoudi group[46,47] and to the low purity of the synthesized phase we obtained, an optimization of the synthesis conditions was realized. RHO-ZMOF was prepared by dissolving 65.3 mmol of 4,5-imidazoledicarboxylic acid (Alfa Aesar) with 32.6 mmol of dehydrated $In(NO_3)_3{\cdot}xH_2O$ (Alfa Aesar) in 500 mL of a 1/1 v/v solution of *N*,*N*-dimethylformamide (DMF)/*N*,*N*-diethylformamide (DEF). A Teflon-lined autoclave of 1 L was filled with the resulting mixture and heated to 426 K for 5 days. The solution was filtered and the product washed with DMF. The low thermal stability (383 K) of the resulting material obliged us to exchange the excess of DMF in the porosity by immerging the as made material in acetonitrile in a PTFE bottle which was heated at 353 K for 1 week.

Purities of all products were verified by XRD (see Supporting Information), thermogravimetric, and N_2 adsorption measurements at 77 K. The results are included in Table 2.

Gas Adsorption Experiments. Adsorption experiments were carried out by using chromatographic methods. Two types of experiments were carried out: (i) single-component pulse experiments at zero coverage and (ii) breakthrough experiments of binary mixtures. A scheme of the apparatus that was used is provided in the Supporting Information. Solvent-wet MOF powder was pressed in a circular mold (diameter of 5 cm) by mechanical force of 4 tons, corresponding to a pressure of ∼200 bar. This procedure offered an acceptable compromise between the mechanical stability of the pellets and the loss of surface area (it decreases by 10−20% due to pelletization). The pellet was broken and sieved to obtain pellets with diameters from 300 to 500 μm. For recording the pulse measurements a stainless steel column of 5.0 cm and an internal diameter of 0.5 cm was filled with 50 mg of pellets. The column was placed in the oven of a chromatograph and heated under a flow of inert gas (helium). The activation conditions of each material are given in the Supporting Information. After activation, the oven was cooled down to the desired adsorption temperature (398 K). Using an injection loop of 250 μL, a pulse of gaseous adsorbate was injected into the column. The elution of the pulse from the column was detected by an FID. Gaseous adsorbate was fed to the injection loop via a flow of helium bubbling through a saturator filled with the liquid adsorbate. The saturator was entirely immersed in a thermostatic bath. Regulation of the temperature of the thermostatic bath and the possibility to dilute with an additional flow of helium allowed us to control the partial pressure in the injection loop.

For recording the binary breakthrough curves the same chromatographic setup as before was used. A longer column was employed to improve the quality of separation (5−7 cm length, ∼600 mg of adsorbent). Instead of using the injection loop, we used a two-way valve to trigger the breakthrough experiment, i.e., to switch from pure helium to helium carrying a binary mixture of hydrocarbons, which was generated by bubbling helium through two separate saturators, each having its own temperature regulation. The column effluent was collected in an injection loop of 250 μL, which was injected at regular intervals into a second GC for analysis. Breakthrough curves were constructed from the GC analysis and corrected from the dead time of the system that was experimentally determined via a breakthrough experiments carried out on a system without a column. Integration of breakthrough curves allowed us to determine the first moment of the curve μ_1 and to calculate adsorbed quantities according to the equation

$$q_{\mathrm{ads},i} = \frac{y_{i,0}}{1 - \sum y_{i,0}} \frac{F_{\mathrm{He}}}{m_{\mathrm{ads}}} \mu_{1,i}$$

where $q_{\mathrm{ads},i}$ is the adsorbed amount of component i, F_{He} the molar flow rate of the carrier gas, m_{ads} the mass of adsorbent, $y_{i,0}$ the molar fraction of component i in the feed, and $\mu_{1,i}$ the first moment of the breakthrough curve of component i. The first moment of the breakthrough curve is calculated from the molar flow rate of component i leaving the column (F_i) via

$$\mu_{i,1} = \int \left(1 - \frac{F_i}{F_{i,0}}\right) \mathrm{d}t$$

The selectivities of adsorption are obtained by the equation

$$\alpha_{i/j} = \frac{q_{\mathrm{ads},i} \cdot y_{j,0}}{q_{\mathrm{ads},j} \cdot y_{i,0}}$$

Except for RHO-ZMOF (which was not heated above 383 K), all the breakthrough experiments were carried out at a temperature of 398 K. The binary mixtures were roughly equimolar. The molar fraction $y_{i,0}$ was between 0.005 and 0.007 in the mixtures without xylenes and between 0.003 and 0.004 in mixtures with xylenes.

A few single-component adsorption−desorption isotherms on ZIF-8 were recorded by gravimetry on a symmetrical TGA system from

dx.doi.org/10.1021/ja211864w | J. Am. Chem. Soc. 2012, 134, 8115−8126

Table 2. Properties of the Materials Tested in This Work

	HKUST-1	CPO-27-Ni	ZIF-8	ZIF-76	RHO-ZMOF	NaY	β
formula	$Cu_3(C_9H_3O_6)_2$	$Ni_2(C_8H_2O_6)$	$Zn(C_4H_5N_2)_2$			$Na_{56}(AlO_2)_{56}(SiO_2)_{136}$	SiO_2
topology	–	–	SOD	LTA	RHO	FAU	BEA
CUS	Cu^{2+}	Ni^{2+}	–	–	–	–	–
counter ions	–	–	–	–	$DMA(H_2O)_X^+$ [a]	Na^+	–
type of porosity	cages	channel	cages	cages	cages	cages	channel
pore diameter/aperture (Å)	12/6.5			18/?			6.7
	10/6.5	11	11.6/3.4	11.6/5.4	18/9	11/7.4	5.6
	6/4.6						
specific surface area (m^2/g)	1842	1423	1813	1561	563	842	687
pore volume (cm^3/g)	0.74	0.54	0.65	0.60	0.22	0.31	0.26
thermal stability (K)[b]	563	633	688	673	383	>773	>773

[a]DMA = dimethylammonium. [b]Determined by TGA experiments in He.

Setaram. As in the breakthrough experiments, a thermostated saturator was used to control the partial pressure of the adsorptives in the He carrier gas. After stabilization of the mass of the solid + adsorbate, the temperature of the saturator was increased stepwise to measure the next point of the isotherm. Once the maximum temperature of the saturator was reached, the procedure was repeated in the backward direction. The objective of these experiments was to detect hysteresis effects in the adsorption−desorption isotherms.

FTIR Spectroscopy. Infrared spectra were recorded on a Nexus Fourier transform instrument equipped with a KBr beam splitter and an MTC nitrogen-cooled detector. A self-supporting pellet of pure powder sample was inserted in a IR cell with KBr windows that was connected to a conventional vacuum/gas manifold. IR spectra were collected in transmission with a resolution of 4 cm^{-1}. Each sample was then pretreated in situ, at 403 K, for 6 h under vacuum ($\sim 10^{-6}$ mbar). The sample was then cooled down to room temperature, and pulses of PX-d_6 or 1-octene were introduced into the IR cell.

^{1}H NMR Spectroscopy. ^{1}H NMR spectra of ZIF-8 sample impregnated with PX were recorded on a Bruker 400 UltraShieldTM spectrometer by using tetramethylsilane as standard. Five portions of around 3 mg of solid were digested in 100 μL of either 250/1000 or 500/1000 v/v solutions of DCl/D_2O 35% wt in DMSO-d_6. The analysis tubes were completed with DMSO-d_6 up to 0.7 mL.

Density Functional Theory (DFT) Calculations. Density functional theory (DFT) calculations were performed using a periodic plane-wave method as implemented in the Vienna Ab initio Simulation Package (VASP 5.2.).[48,49] The exchange−correlation functional was treated within the generalized gradient approximation (GGA) parametrized by Perdew, Burke, and Ernzernhof (PBE),[50] and the electron-ion interaction was described by the projector augmented wave (PAW) scheme[48] with an energy cutoff of 400 eV. Spin-polarized calculations were performed, using the interpolation formula of Vosko, Wilk, and Nusair.[51] Dispersion corrections were systematically included to energies and geometries (forces), within the DFT-D2 method of Grimme.[52] Full optimization of structures was performed, until forces on each atom in each direction were inferior to 2×10^{-2} eV $Å^{-1}$. The unit cell of CPO-27-Ni was doubled in the c direction before simulating the adsorption of PX or 1-octene. The conventional cell of HKUST-1 was used for the calculations. Energies were calculated at the gamma point.

RESULTS

In order to facilitate the interpretation of the results, we briefly describe the selected MOF structures and then sum up the main separation mechanisms in the following sections.

Brief Description of the MOF Structures. Important characteristics of the selected MOFs are summarized in Table 2. Their structures are shown in the Supporting Information. Briefly, Cu-btc (HKUST-1)[53,54] has a three-dimensional pore structure with three types of cages. The smallest cages, commonly named "side pockets" have an aperture of 4.6 Å and an internal diameter of ~6 Å. The arrangement of eight side pockets at the corners of a cube forms two types of big cages with internal diameters of 10 and 12 Å. The aperture between the large cages has a diameter of 6.5 Å. The pore structure is generated by the connection of dimeric clusters of copper coordinated with four carboxylate groups of trimesic acid. In the as-synthesized material, the axial ligand on the Cu-dimer is occupied by a water molecule that can be removed by heating, thereby creating a CUS.

In CPO-27-Ni,[43] six linear and parallel chains, made up of NiO_6 edge-shared octahedra, are interconnected by fully deprotonated dihydroxy-terephtalate moieties, resulting in a honeycomb structure. The one-dimensional channels have a diameter of 11 Å and, like in Cu-btc, one of the two axial ligands of Ni^{2+}, which is a water molecule, can be removed by heating, creating a CUS.

In ZIF-8,[55,56] zinc cations are coordinated to four 2-methylimidazolate ligands, resulting in a hybrid material with sodalite topology (SOD). The sodalite cages possess a pore diameter of 11.6 Å and the aperture between two cages is 3.4 Å. Note that the formal size of the aperture is smaller than the size of most hydrocarbons, but it was recently shown that ZIF-8 can adsorb n-alkanes whose kinetic diameter is 4.3 Å.[57]

ZIF-76[58] is generated by the association of imidazole and 5-chlorobenzimidazole linkers with Zn^{2+} cations, resulting in a hybrid material with the zeolite topology LTA. In this topology, sodalite cages (at the corners of a cube) are connected by double-four rings, which generates a large supercage in the center of the unit cell. The 6-membered ring windows of the sodalite cages are only occupied by imidazolate ligands; therefore, the pore aperture is larger than in ZIF-8, i.e., 5.2 Å. The large supercage is accessible through 8-ring apertures. The 5-chlorobenzimidazolate ligands (ClbIm) point toward the opening of the pore (if the distribution is regular, there are two ClbIm ligands per 8-ring), making it difficult to measure precisely the diameter of the 8-ring aperture of this cage. In any case, all apertures of ZIF-76 are larger than in ZIF-8.

Finally, RHO-ZMOF[46] is also a zeolitic imidazolate framework where In^{3+} cations are connected by 4,5-dicarboxyimidazolate ligands. The carboxylic acid substituents of the imidazole ring are deprotonated. One of the two carboxylates coordinates to In^{3+}; the other is free and lends a negative charge to the framework, which is compensated by an extraframework cation. In the as synthesized form the extraframework cation is the dimethylammonium cation DMA^+, generated by the decomposition of the solvent N,N-dimethylformamide during the synthesis.[47]

dx.doi.org/10.1021/ja211864w | J. Am. Chem. Soc. 2012, 134, 8115−8126

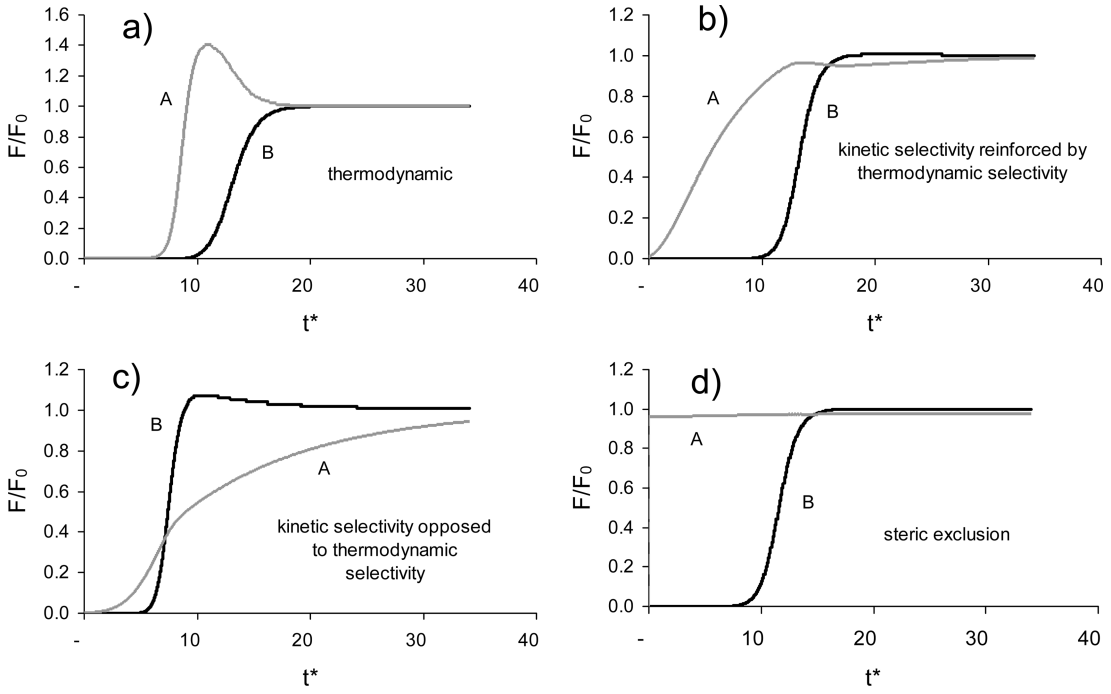

Figure 1. Examples of binary breakthrough curves: (a) case of thermodynamic selectivity, (b) case of kinetic selectivity reinforced by thermodynamic selectivity, (c) case where kinetic and thermodynamic selectivities are opposed, and (d) steric exclusion of one of the components. The time axis is dimensionless (time divided by contact time).

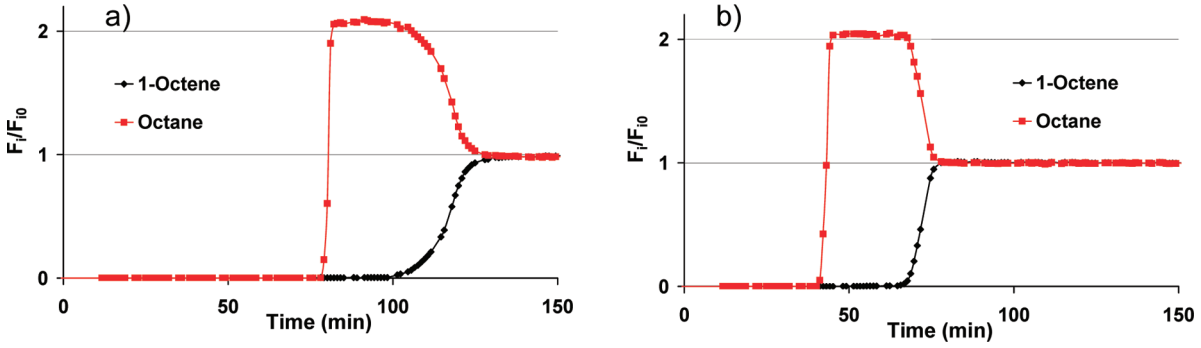

Figure 2. Breakthrough curves of the 1-octene/*n*-octane mixture on (a) HKUST-1 and (b) NaY at 398 K. $P(=C8)$ = 600 Pa; $P(nC8)$ = 470 Pa.

Separation Mechanisms. Adsorptive separations can be classified in three different kinds of mechanisms, namely, thermodynamic, kinetic, and steric.

Thermodynamic separations can be based on enthalpic or entropic effects or a combination of both. In the case of an enthalpic separation, the molecule that has the strongest interaction with the framework is preferentially retained by the adsorbent. While enthalpic separations are the general rule, there are some cases where molecules having very similar adsorption enthalpies can be separated thanks to entropy. Entropy-based adsorption selectivity may arise from the fact that one of the adsorbed molecules retains more internal degrees of freedom or that the molecule has access to a larger number of configurations in the adsorbed phase (a larger number of "adsorption sites"). Prominent examples are the separation of xylene isomers by faujasite zeolites,[59] the preferential adsorption of linear alkanes in silicalite-1,[60−62] and the phenomenon of inverse shape selectivity.[63]

The kinetic separation of molecules is based on the difference of the diffusion rate of two molecules in the porosity of the adsorbent. The molecule with the larger diffusion constant migrates faster into the core of the adsorbent particles and is the most adsorbed molecule. Note that kinetic selectivity may only be transitory. It can be overruled or enhanced by a thermodynamic selectivity when sufficient time is given to the system to approach equilibrium. The steric separation is an extreme case of a kinetic separation where the diffusion rate of one of the molecules is quasizero. Steric selectivity, or size exclusion, happens when the critical diameter of a molecule is larger than the pore aperture, thereby hindering the molecule from penetrating into the porosity of the adsorbent. The molecule is, therefore, quickly eluted from the adsorption column.

Breakthrough curves are a very good means to distinguish the above-mentioned separation mechanisms, because each of them has some characteristic features. Thermodynamic separations without any diffusional limitations are characterized by very sharp breakthrough fronts and a marked roll-up. Roll-up means that the flow rate of the more weakly adsorbed component A, which elutes first from the column, becomes momentarily higher than the feed flow rate (see Figure 1). It happens when molecule A that was adsorbed at the end of the

dx.doi.org/10.1021/ja211864w | J. Am. Chem. Soc. 2012, 134, 8115−8126

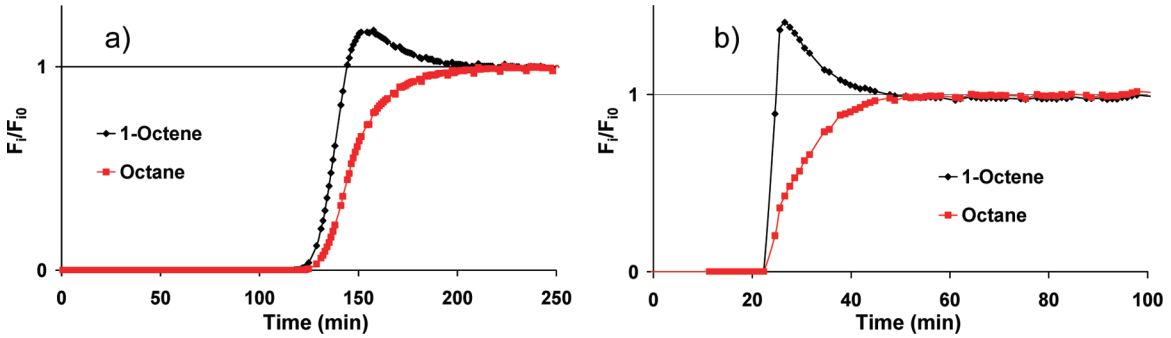

Figure 3. Breakthrough curves of the 1-octene/*n*-octane mixture on (a) ZIF-76 [P(=C8) = 300 Pa, P(*n*C8) = 350 Pa] and (b) siliceous zeolite β [P(=C8) = 740 Pa, P(*n*C8) = 550 Pa] at 398 K.

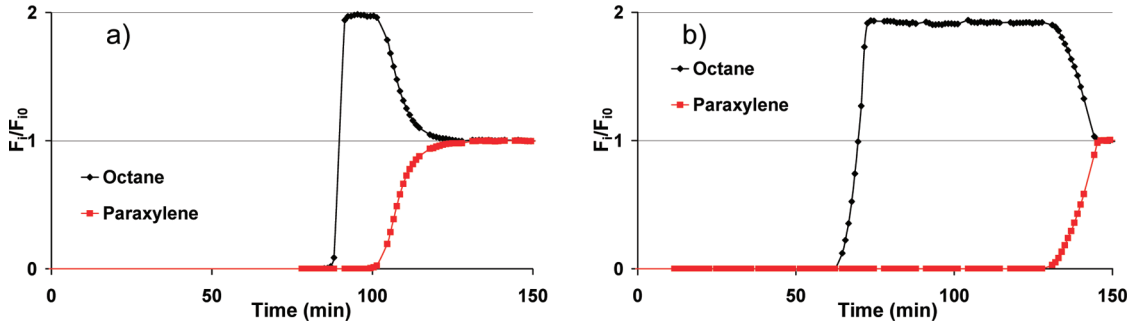

Figure 4. Breakthrough curves of the *n*-octane/PX mixture on (a) HKUST-1 and (b) NaY at 398 K. P(*n*C8) = 315 Pa, P(PX) = 385 Pa.

column is desorbed by competitive adsorption of the more strongly adsorbed molecule B, when the concentration front of B, which advances more slowly through the column, arrives.

Diffusional limitations render the concentration fronts more dispersed. Since kinetic separations are based on diffusional limitations, the breakthrough profiles of kinetic separations are necessarily less sharp. Since the molecules have troubles diffusing into the core of the adsorbent particles, breakthrough may occur quite early and it takes a long time to reach the plateau of the breakthrough curve. If thermodynamic selectivity is opposed to kinetic selectivity, the two breakthrough curves may cross each other. Roll-up also occurs in kinetic separations, but it is smeared out because the displacement of molecule A by molecule B is not very quick.

In the extreme case of total steric exclusion of molecule A, molecule A elutes immediately from the column, and since it was not at all adsorbed, there is also no roll-up.

Separation of Alkene/Alkane Mixtures. The order of elution of a 1-octene/octane mixture strongly depends on the polarity of the adsorbent. Polar materials with unsaturated metal centers or extraframework cations (HKUST-1, CPO-27-Ni, and NaY) preferentially adsorb 1-octene thanks to the specific interaction between the double bond of alkenes and the metal centers or extraframework cations (Figure 2), as will be illustrated by DFT (vide infra).

Materials with apolar frameworks display the opposite trend. ZIF-8, ZIF-76, and siliceous zeolite β adsorb octane preferentially (Figure 3). The alkane has a higher boiling point than the alkene; therefore, the preferential adsorption of octane agrees with the expected order of elution in the absence of any specific adsorbate/adsorbent interactions.

In all cases, the rather sharp breakthrough fronts and the marked roll-up suggest that the origin of the selectivity is thermodynamic.

Separation of Alkane/Aromatics Mixtures. As for the alkane/alkene separation, the order of elution of the octane/PX mixture depends on the polarity of the adsorbent. Polar materials as HKUST-1, CPO-27-Ni, RHO-ZMOF, and NaY preferentially adsorbed PX over *n*-octane (Figure 4). The unsaturated metal centers or the extraframework cations seem to preferentially interact with the aromatic ring of the PX molecule.

Apolar materials, i.e., ZIF-8, ZIF-76, and zeolite β, preferentially adsorb *n*-octane compared to PX (Figure 5). In this case, it is not possible to link the order of elution to the boiling point of the adsorbate. PX has a higher boiling point than *n*-octane, but *n*-octane is preferentially adsorbed.

The shape of the breakthrough curve of the PX on the ZIF-8 indicates strong diffusional limitations, but there is no neat steric exclusion. PX can enter into the porosity, albeit with difficulty, in spite of the fact that its kinetic diameter is almost twice as large as the formal pore size of ZIF-8 (6.7 vs 3.4 Å)!

Separation of Alkene/Aromatic Mixtures. For the separation of 1-octene/PX, materials with extraframework cations (NaY and RHO-ZMOF) preferentially adsorb the aromatic molecule (Figure 6). Inversely, materials with coordinatively unsaturated metal sites (HKUST-1 and CPO-27-Ni) or apolar frameworks (ZIF-8 and zeolite β) preferentially adsorb the alkene rather than the aromatic compound, in spite of the higher boiling point of the latter (Figure 7). The shape of the breakthrough curves indicates that the origin of the para-selectivity is kinetic in the case of ZIF-8 but thermodynamic for the CUS-MOFs and for zeolite β. Note that this is the only separation studied in this work where the selectivity of MOFs with coordinatively unsaturated metal sites differs from that of adsorbents with extraframework cations. We will come back to this point in the discussion.

dx.doi.org/10.1021/ja211864w | *J. Am. Chem. Soc.* 2012, 134, 8115−8126

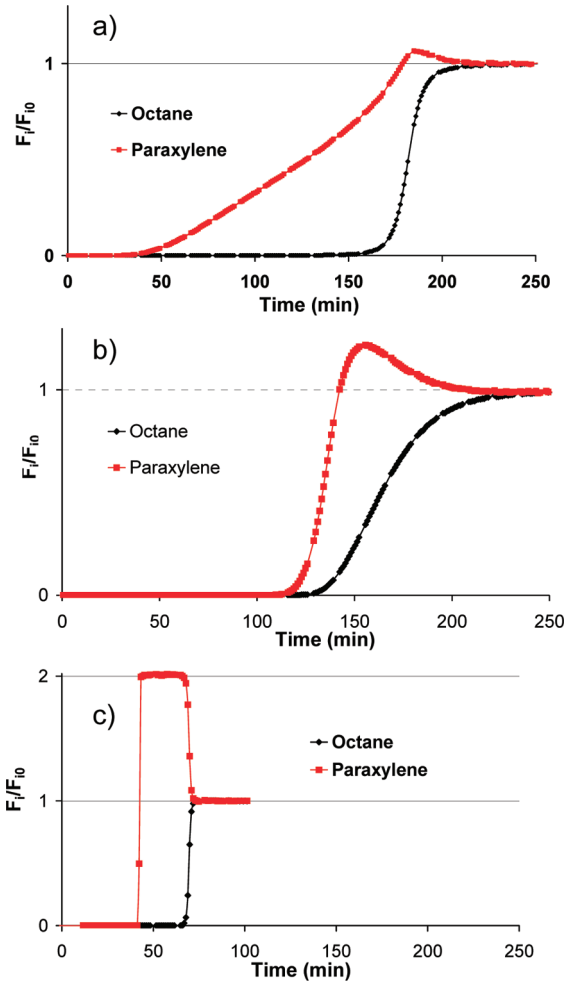

Figure 5. Breakthrough curves of the *n*-octane/PX mixture on (a) ZIF-8, (b) ZIF-76, and (c) siliceous zeolite β at 398 K. P(*n*C8) = 305 Pa, P(PX) = 385 Pa.

Separation of OX/PX. The molecular properties that distinguish *o*- and *p*-xylene isomers are the dipole moment and the critical diameter. The two molecules can therefore be separated on the basis of polarity of the adsorbent or on pore size effects.

RHO-ZMOF, NaY, HKUST-1, CPO-27-Ni, and also the apolar adsorbent ZIF-76 are ortho-selective, i.e., the order of elution of the ortho/para isomers follows the order of their dipole moments or boiling points. Figure 8 shows as examples the breakthrough curves of the most and the least ortho-selective adsorbents, i.e., CPO-27-Ni and ZIF-76, respectively. Only the siliceous zeolite β and ZIF-8 were para-selective (Figure 9). As in the previous examples, the shape of the breakthrough curves indicates that the origin of the para-selectivity is kinetic in the case of ZIF-8, but this is clearly not the case for the zeolite β (marked roll-up and sharp breakthrough fronts).

Summary. Table 3 summarizes the adsorbed quantities and selectivities obtained for all binary mixtures on each material.

NaY and RHO-ZMOF, the two materials with extraframework cations, adsorb the model compounds in the order aromatic > alkene > alkane. NaY is a lot more selective than RHO-ZMOF. In the separation of the xylene isomers, both prefer the more polar compound OX. In the case of HKUST-1 and CPO-27-Ni, the order of elution is alkane < aromatic < alkene, i.e., the alkene/aromatic affinity was inversed compared to NaY. The apolar adsorbents ZIF-8, ZIF-76, and zeolite β have their order of elution reversed with respect to NaY, i.e., alkane > alkene > aromatic. The selectivity is of kinetic nature in the case of ZIF-8 but clearly of thermodynamic nature in the case of zeolite β and ZIF-76.

DISCUSSION

Gate Opening Effects in ZIF-8. Our binary adsorption experiments have shown that ZIF-8 separates *n*-octane and 1-octene from *p*-xylene by molecular sieving. The diffusion of PX into the pores of ZIF-8 is much slower than that of *n*-octane or 1-octene, because of the larger kinetic diameter of PX. Still, PX is not entirely excluded from the pore system, although its kinetic diameter is almost twice as large as the formal pore size of ZIF-8. The formal pore size of ZIF-8 should not even allow *n*-octane and 1-octene to enter into the pore system because their kinetic diameters are also larger than 3.4 Å, but the sharp breakthrough fronts of *n*-octane and 1-octene prove that both can readily diffuse into ZIF-8. Indeed, inverse gas chromatography experiments have already shown that ZIF-8 readily adsorbs *n*-alkanes.[4,5] The easy passage of *n*-octane and 1-octene across the narrow pore aperture of ZIF-8 indicates that the aperture must be quite flexible and has the possibility to open up in order to allow molecules to pass into sodalite cage. Moggach et al. have shown that a strong mechanical pressure (1.4 GPa) induces a rotation of the ZIF-8 ligands, which increases the pore aperture from 3.4 to 4.5 Å.[31] The latter diameter would be sufficiently large to explain the adsorption of *n*-octane and 1-octene, but the pressure in our experiments is orders of magnitude lower than 1.4 GPa. Recent work by Fairen-Jimenez et al. revealed, however, that adsorption can have the same effect as mechanical pressure.[32] The phase

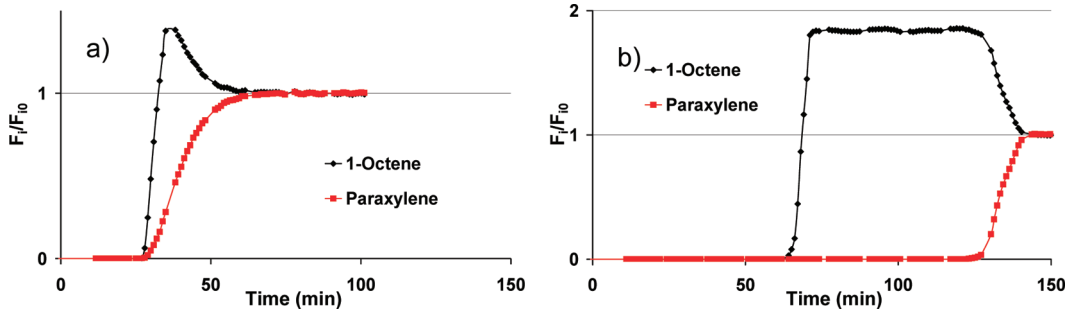

Figure 6. Breakthrough curves of the 1-octene/PX mixture on (a) RHO-ZMOF [P(=C8) = 310 Pa, P(PX) = 260 Pa] and (b) NaY [P(=C8) = 320 Pa, P(PX) = 330 Pa] at 398 K.

dx.doi.org/10.1021/ja211864w | J. Am. Chem. Soc. 2012, 134, 8115–8126

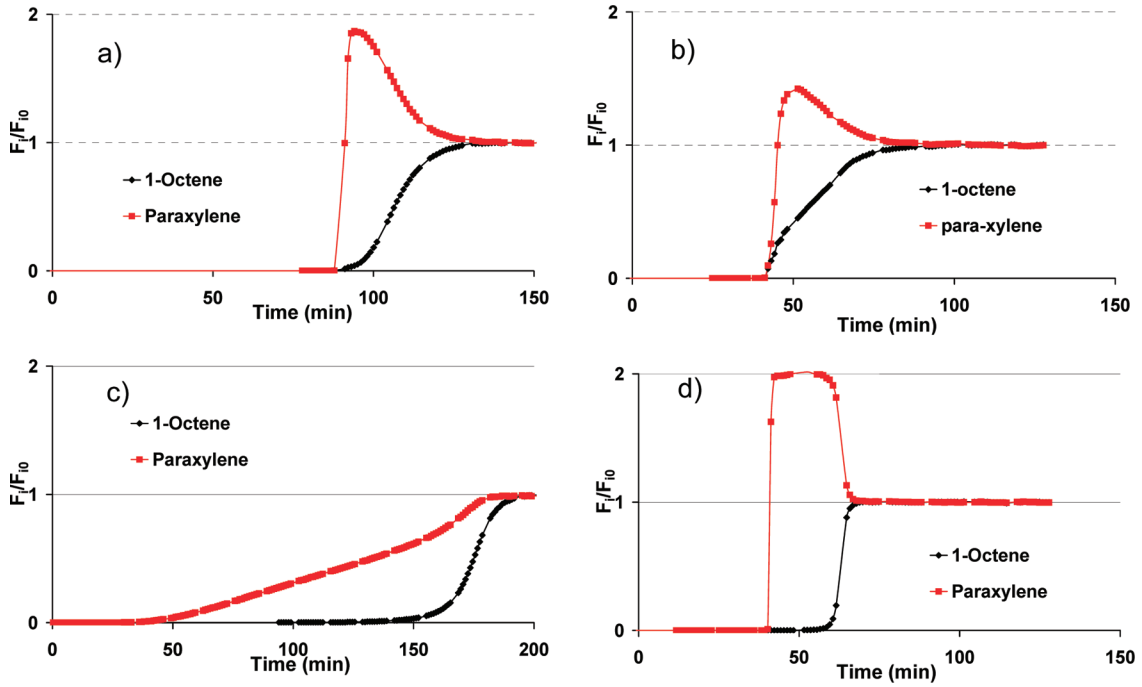

Figure 7. Breakthrough curves of the 1-octene/PX mixture on (a) HKUST-1, (b) CPO-27-Ni, (c) ZIF-8, and (d) zeolite β at 398 K. P(=C8) = 300 Pa, P(PX) = 380 Pa.

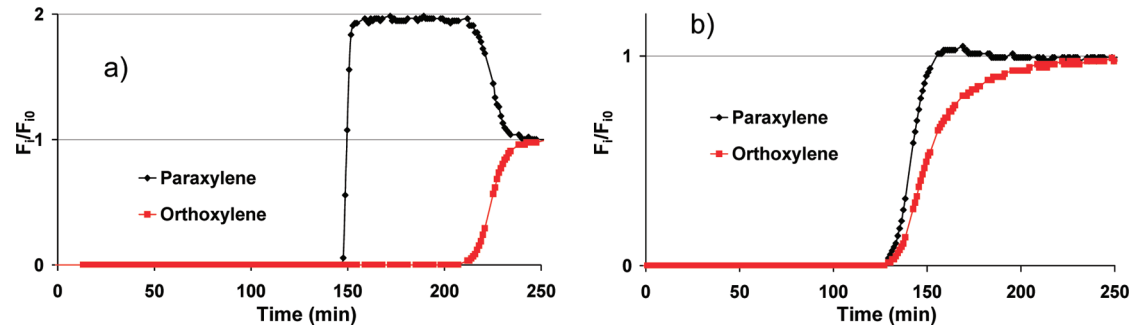

Figure 8. Breakthrough curves of the OX/PX mixture on (a) CPO-27-Ni and (b) ZIF-76 at 398 K. P(OX) = 320 Pa, P(PX) = 280 Pa.

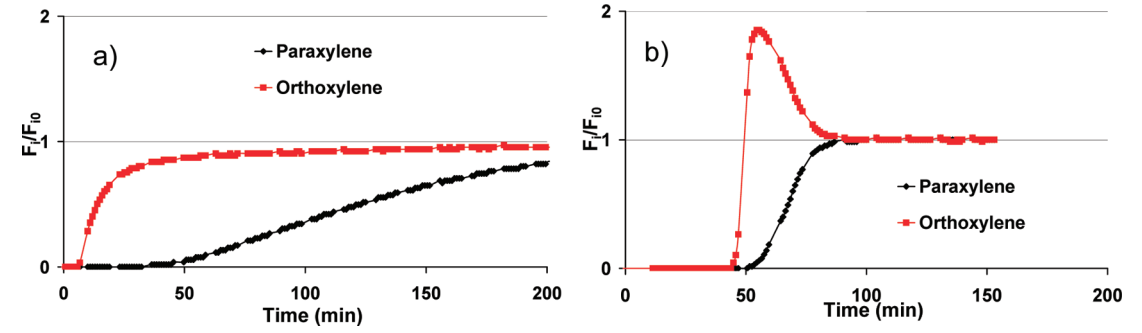

Figure 9. Breakthrough curves of the OX/PX mixture on (a) ZIF-8 and (b) zeolite β at 398 K. P(OX) = 320 Pa, P(PX) = 260 Pa.

transition of ZIF-8 could simply be induced by filling the pores of ZIF-8 by N_2 molecules at 77 K, at a pressure lower than 100 kPa. We may suppose that a similar phenomenon is happening during the adsorption of *n*-octane and 1-octene. This previously observed structural flexibility of ZIF-8 is, however, still insufficient to explain the adsorption of PX. In order to investigate what happens to the structure of ZIF-8 when it adsorbs PX, we filled the pores of ZIF-8 with PX in the liquid phase under a pressure of 2.2 MPa, in order to maximize the driving force, and a temperature of 448 K, in order to promote diffusion. The solid was then dried in a flow of N_2 at room temperature in order to remove PX from the outer surface. ^{1}H NMR analysis of ZIF-8 material impregnated with PX performed after digestion of the sample with DCl/D_2O 35 wt % solution in DMSO-d_6 revealed that the average PX/2-methylimidazole ratio is 0.30, which corresponds to 3.6 molecules of PX remained adsorbed per sodalite cage. Contrary to the results of Fairen-Jimenez et al., the XRD pattern of the

dx.doi.org/10.1021/ja211864w | *J. Am. Chem. Soc.* 2012, 134, 8115−8126

Table 3. Adsorbed Quantities and Selectivities Obtained from Integration of the Breakthrough Curves[a]

		NaY	HKUST-1	CPO-27-Ni	RHO ZMOF	ZIF-8	ZIF-76	siliceous zeolite β
				=C8/*n*C8				
=C8	mmol cm^{-3}	2.11	2.18	1.78	0.45	0.55	0.18	0.93
*n*C8	mmol cm^{-3}	0.32	0.61	0.55	0.45	0.59	0.24	1.02
selectivity		5.4	2.7	3.8	1.0	0.9	0.9	0.7
				PX/*n*C8				
PX	mmol cm^{-3}	2.63	1.76	0.76	0.68	0.38	0.15	0.26
*n*C8	mmol cm^{-3}	0.08	1.00	0.40	0.48	0.73	0.22	1.32
selectivity		27.2	1.5	1.6	1.5	0.7	0.8	0.2
				PX/=C8				
PX	mmol cm^{-3}	2.22	1.21	0.59	0.59	0.39	0.15	0.33
=C8	mmol cm^{-3}	0.22	1.51	0.71	0.44	0.69	0.22	1.22
selectivity		9.6	0.7	0.7	1.6	0.7	0.9	0.3
				OX/PX				
PX	mmol cm^{-3}	0.92	1.20	0.86	0.63	0.47	0.18	1.31
OX	mmol cm^{-3}	1.80	1.63	2.93	0.92	0.15	0.26	0.72
selectivity		1.4	1.3	3.3	1.3	0.3	1.1	0.5

[a] *n*C8, octane; =C8, octene; PX, *p*-xylene; OX, *o*-xylene.

PX/ZIF-8 product (see Supporting Information) was not significantly different from that of the parent ZIF-8 (no symmetry loss), although the relative intensities of the diffraction peaks change upon impregnation, thereby proving indirectly the presence of PX inside the sodalite cage. The phase transition of ZIF-8 observed by Fairen-Jimenez et al. is due to adsorption of N_2 in the aperture of the sodalite cage. Larger molecules like PX cannot be hosted inside the aperture. We therefore suppose that the opening of the aperture, which allows the transition of PX, is only transitory.[64] One can make the analogy with a saloon door that opens when the molecule passes and closes again when they have entered the sodalite cage. We estimated that a complete (transitory) tilt of the 2-methylimidazolate ligands—in that case the pore aperture diameter of the ZIFs is not any more limited by the methyl hydrogen atoms but by the nitrogen atoms of the aromatic ring—would result in a pore aperture of 6.4 Å, which is close to the kinetic diameter of the PX.

Gate-opening effects have already been observed in other ZIFs, in particular, ZIF-7 and ZIF-9, which are nonporous in N_2 adsorption experiments at 77 K but adsorb CO_2 or light hydrocarbons at room temperature above a certain gate-opening pressure.[24,65−67] The isotherms of gate-opening ZIFs are characterized by a steep step and a strong hysteresis upon desorption. Figure 10 shows the isotherms of *n*-octane and PX on ZIF-8 at 398 K. The isotherm of *n*-octane has a classical concave shape and has no hysteresis; i.e., it shows no sign of gate-opening in the pressure range of our study. The isotherm of PX is curved upward, i.e., convex, which may be interpreted as an isotherm with a very diffuse step, but there is again no hysteresis. The absence of hysteresis confirms that we are not dealing with a phase transition of ZIF-8, as is the case in most ZIFs/MOFs where gate-opening effects were observed, but only with a transitory deformation of the pore aperture that allows molecules to go in and out.

Apolar Adsorbents. The order of elution of molecules on nonspecific chromatographic columns strongly depends on the boiling point of the adsorbate. Thus, for our model compounds, the expected order of elution would be 1-octene < octane < PX. For the three apolar materials ZIF-8, ZIF-76, and siliceous β, the observed order of elution is PX < 1-octene < octane. The highest boiling molecule, PX, is systematically the least

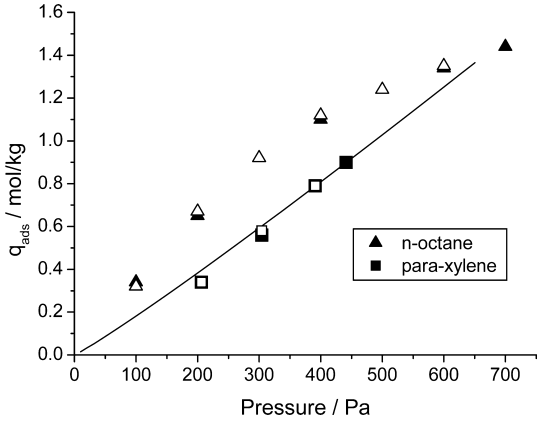

Figure 10. Adsorption isotherms of *n*-octane and PX at 398 K, measured by gravimetry. Full symbols present the adsorption branch and open symbols the desorption branch. The line presents the isotherm of PX obtained by breakthrough experiments, for comparison.

adsorbed. In the case of ZIF-8, the reason for the quick elution of PX is diffusional limitation, but the isotherms in Figure 10 confirm that PX is indeed more weakly adsorbed than *n*-octane. For ZIF-76 and siliceous β, the selectivity is clearly of thermodynamic nature. The order of elution PX < 1-octene < octane is also found for the injection of pulses, i.e., at very low coverage (Supporting Information). The order of elution is therefore not the result of packing and confinement effects at higher coverage.

A decrease of the magnitude of the adsorption enthalpy from octane to PX was already observed on MIL-47,[9] a non-CUS MOF. The effect was attributed to H-bonding interactions between the alkane chain and oxygen atoms of the ligand (terephtalate). This explanation does, however, not apply to ZIFs. We therefore believe that the order of adsorption, octane >1-octene > PX, can be explained by the flexibilities of the molecules, which increase in the same order. The high flexibility of aliphatic chains may help to maximize the adsorption enthalpy, by allowing the molecule to fit closely to the wall of the framework and to optimize the van der Waals interactions. It may also play a beneficial role for the adsorption entropy, by allowing a molecule to occupy a larger number of favorable

configurations in the adsorbed phase. Our data does not allow us to distinguish enthalpic from entropic effects, but we can evoke the work of Finsy et al.,[9] who found that the adsorption enthalpy of *n*-octane on MIL-47, which can also be considered as an unpolar MOF, is higher than that of xylene isomers. The octane/PX selectivity is much higher in zeolite β than in the large cages of the ZIF materials because the confinement is stronger.

Concerning the separation of OX and PX, ZIF-8 and zeolite β are para-selective while ZIF-76 is ortho-selective. The ortho-selectivity of ZIF-76 corresponds to the normally expected behavior; the para-selectivity of ZIF-8 results from molecular sieving and that of zeolite β must be the consequence of a preferential arrangement of PX in the pores.

Polar Adsorbents. The polarity of the framework induced by counterions or unsaturated metal centers allows specific interactions with the unsaturated molecules. In an electrostatic picture, the reason for these specific interactions is that double bonds have electric multipole moments, which interact with the electric field in the adsorbent. The expected order of adsorption in polar adsorbents is, therefore, OX > PX > 1-octene > octane. This order is indeed found in materials that have counterions, i.e., RHO-ZMOF and NaY. NaY is systematically more selective than RHO-ZMOF because the electric field generated by the "hard" cation Na^+ is much stronger than that of the soft hydrated DMA^+ cation [the poor thermal stability of the RHO-ZMOF (383 K) does not allow the dehydration of the dimethylammonium ion].[47] The effect may be reinforced by the smaller pore size of NaY compared to RHO-ZMOF.

However, the two MOFs with unsaturated metal centers (HKUST-1 and CPO-27-Ni) preferentially adsorb 1-octene over PX. The order of elution PX < 1-octene was also found in pulse experiments at close to zero coverage (see Supporting Information). Therefore, the order of elution is not related to effects of preferential arrangement at high pore filling.

We used FTIR spectroscopy to investigate the interaction of 1-octene and PX with the unsaturated metal centers in HKUST-1 and CPO-27-Ni in more detail. Figure 11 shows the spectra of CPO-27-Ni; results for HKUST-1 were very similar. We can observe that all aliphatic CH-stretching vibrations of 1-octene (in the range of 3000−2850 cm^{-1} in the gas phase) are shifted by 12−18 cm^{-1} to lower wavenumbers when the molecule adsorbs on CPO-27-Ni.

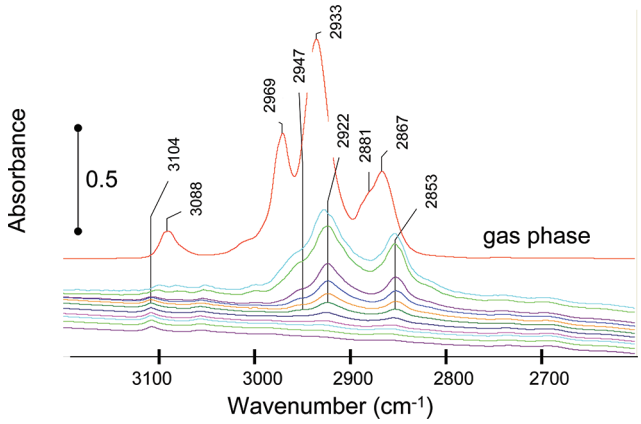

Figure 11. FTIR difference spectra of 1-octene adsorbed on CPO-27-Ni, at room temperature. The trace on top is the gas-phase spectrum of 1-octene.

The CH-stretching vibration of the double bond, however, shifts to higher wavenumbers (from 3086 to 3104 cm^{-1}). This shift is consistent with a π-bonding between octene and the Ni^{2+} cation. Back-donation from Ni^{2+} weakens the C=C double bond but at the same time strengthens (i.e., shortens) the C−H bond,[68] which explains the hypsochromic shift of the C−H vibration. On the contrary, no significant shift of the CD-stretching vibrations of deuterated PX-d_6 was observed, which implies that there was no intimate interaction between the methyl groups and the framework. For comparison, adsorption of PX on NaY leads to a band shift of the CH_3-stretching vibrations of 10−15 cm^{-1} to lower wavenumbers.[69]

To investigate the subject further, the nature of the interaction between PX or 1-octene and the unsaturated metal centers of CPO-27-Ni was addressed by DFT calculations. The results of the geometry optimization of the adsorbed structure on CPO-27-Ni are shown in Figure 12. Table 4 reports the adsorption energies and C···Ni distances. Note that for the adsorption of PX in CPO-27-Ni, we also found a stable adsorption mode in which the metal center is not involved, that is, π-stacking with the linker. This mode is shown in the Supporting Information and does not modify the conclusions presented here.

It appears that 1-octene can approach the unsaturated metal centers much more closely than the PX molecule. As a consequence, the aromatic molecule is unable to form any covalent bond with nickel, so that the interaction between the molecule and the framework remains purely dispersive. On the contrary, 1-octene shares some electrons with nickel, a coordination bond is formed with atoms belonging to the C=C double bond of the molecule. This is shown by (i) the fact that the interaction is not fully dispersive (Table 4) and (ii) the bond overlap population calculations (performed with CASTEP), which show nonzero population for both C−Ni bonds (C belonging to the C=C double bond). Calculations performed on HKUST-1 (see Supporting Information) denote the same trend.

From the combined information on DFT and IR spectroscopy, we can conclude that the relatively weak interaction of aromatics with coordinatively unsaturated metal sites arises from a problem of accessibility. The interaction between an alkene and the CUS is stronger because the linear alkene is less sterically hindered and can therefore approach more closely the metal center and form a covalent coordination bond. This flexibility argument is further supported by data of Maes et al.,[14] who showed that HKUST-1 adsorbed vinylcyclohexane less strongly than ethylbenzene. Vinylcyclohexane is less flexible and sterically more demanding than 1-octene and presumably cannot approach the CUS site as easily. In that case, the adsorption of the aromatic molecule is preferred over that of the olefin. The problem of accessibility does not arise in materials with extraframework cations, i.e., NaY and RHO-ZMOF, because the cations are more exposed. Moreover, the extraframework cations can, if necessary, be pulled away from their equilibrium position in the empty framework to optimize the interaction with the aromatic ring.[37]

■ CONCLUSIONS

Our study of the coadsorption of C8 aromatics, alkenes, and alkanes has unveiled some general trends in the separation of hydrocarbons by MOFs but also some original properties. In particular, it has revealed remarkable molecular sieving properties for ZIFs. In contrast to zeolites, where pore

dx.doi.org/10.1021/ja211864w | J. Am. Chem. Soc. 2012, 134, 8115−8126

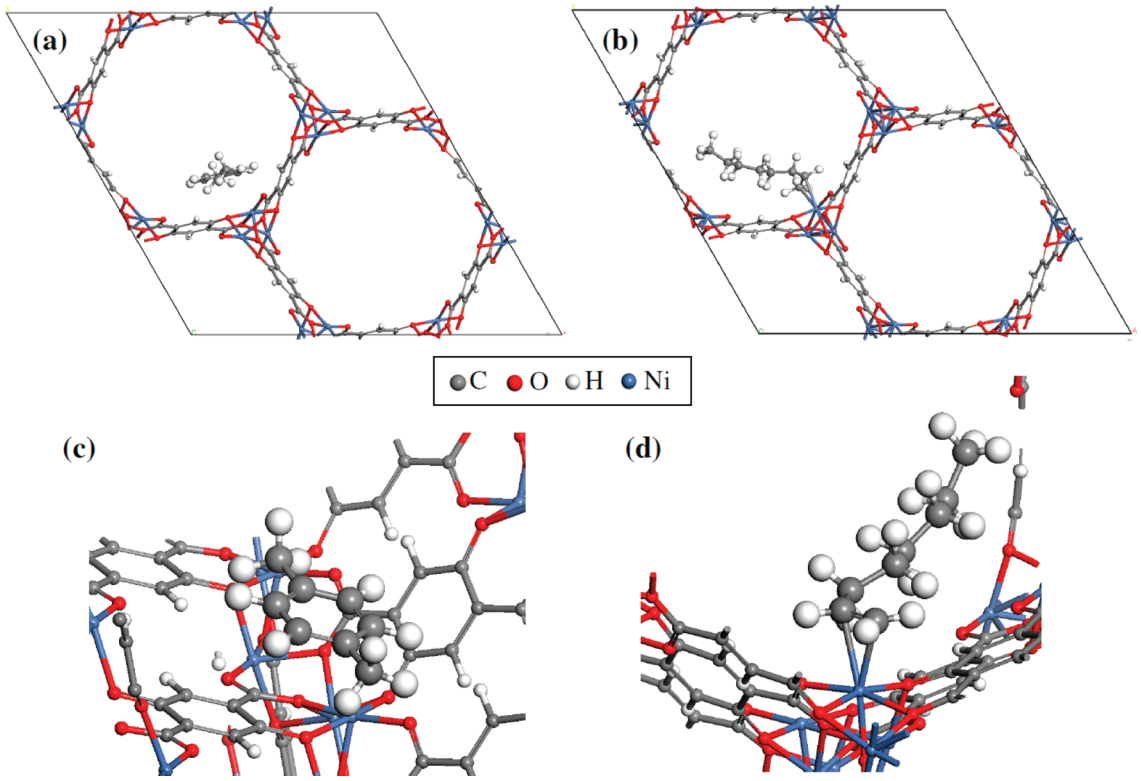

Figure 12. Geometries of CPO-27-Ni optimized by DFT+D calculations for the adsorption of (a) PX and (b) 1-octene. Parts c and d are magnifications of parts a and b, respectively.

Table 4. Adsorption Energies (including dispersion corrections) and C···Ni Distances Calculated by DFT of PX and 1-Octene on Metallic Sites of CPO-27-Ni

	total adsorption energy ($kJ \cdot mol^{-1}$)	dispersive component (%)	C···Ni (Å)[a]
p-xylene	−90	100	3.667
1-octene	−122	85	2.340

[a]For the PX molecule, the C···Ni distance corresponds to the average distance between the metallic center and each of the six carbon atoms of the aromatic ring. For the 1-octene molecule, it relates to the average distance between the metallic center and each carbon atom of the double C=C bond.

openings are rather rigid, the molecular sieving feature of ZIFs is strongly related to the flexibility of the pore aperture. In the case of ZIF-8, a transitory tilt of the imidazolate ligands allows increasing the effective pore opening by almost a factor of 2 and enables the passage of molecules as large as PX, although the formal pore size is only 3.4 Å. Although it is not yet well understood why some ZIFs can exhibit such a tremendous flexibility of the pore open, this feature opens unexpected possibilities for the use of these materials in the separation of large molecules. In parallel work we have, for example, shown that some ZIFs can perform better than zeolite 5A in the separation of paraffin isomers, because they combine excellent molecular sieving properties with high adsorption capacities, because of their high pore volume.[70]

If the pore size of a ZIF is too large to exhibit molecular sieving properties and if the ZIF does not carry highly polar functional groups, it behaves like an apolar adsorbent, i.e., it adsorbs in the order alkane > alkene > aromatic.

On the other hand, MOFs with coordinatively unsaturated sites behave like polar adsorbents (zeolites with extraframework cations) with one exception: they preferentially adsorb alkenes with flexible side chains over aromatics. Normally, the π-electrons of the aromatic ring interact strongly with extraframework cations and are more strongly adsorbed than alkenes, but in the case of coordinatively unsaturated sites, which form part of the metal−organic framework, the approach of the aromatic ring to the metal site is sterically hindered by the surrounding ligands and this considerably weakens the interaction. Such a steric hindrance does not occur for linear alkenes. A covalent coordination bond with the unsaturated metal center is even formed.

Finally, MOFs with extraframework cations behave qualitatively like their analogous zeolites, as the accessibility of the adsorption site and the rules governing the adsorption (mainly electrostatic) are similar.

Thanks to the understanding of the rules governing adsorption in various kinds of MOF materials, this work will help one to choose the type of MOF that is best suited for obtaining the desired selectivity in a given hydrocarbon separation problem. The choice between zeolite or MOF adsorbents will always depend on the specific application (required purity of the products, temperature of operation, economics), but a general advantage of MOFs is that many of them have a higher pore volume than zeolites and, therefore, a potentially higher adsorption capacity.

■ ASSOCIATED CONTENT

Supporting Information

Structures of the adsorbents used in this work, experimental details of the breakthrough measurements, and details of the DFT calculations. This information is available free of charge via the Internet at http://pubs.acs.org/.

AUTHOR INFORMATION

Corresponding Author

gerhard.pirngruber@ifpen.fr

Notes

The authors declare no competing financial interest.

ACKNOWLEDGMENTS

The authors gratefully acknowledge E. Sorbier (IFPEN) for carrying out the IR experiments. Calculations were performed at IFPEN HPC center and at IDRIS/CINES HPC center (project x2011086134 funded by GENCI).

REFERENCES

(1) Pan, L.; Olson, D. H.; Ciemnolonski, L. R.; Heddy, R.; Li, J. *Angew. Chem., Int. Ed.* **2006**, *45*, 616−619.

(2) Chen, B. L.; Liang, C. D.; Yang, J.; Contreras, D. S.; Clancy, Y. L.; Lobkovsky, E. B.; Yaghi, O. M.; Dai, S. *Angew. Chem., Int. Ed.* **2006**, *45*, 1390−1393.

(3) Barcia, P. S.; Zapata, F.; Silva, J. A. C.; Rodrigues, A. E.; Chen, B. *J. Phys. Chem. B* **2007**, *111*, 6101−6103.

(4) Luebbers, M. T.; Wu, T.; Shen, L.; Masel, R. I. *Langmuir* **2010**, *26*, 15625−15633.

(5) Chang, N.; Gu, Z. Y.; Yan, X. P. *J. Am. Chem. Soc.* **2010**, *132*, 13645−13647.

(6) Barcia, P. S.; Guimaraes, D.; Mendes, P. A. P.; Silva, J. A. C.; Guillerm, V.; Chevreau, H.; Serre, C.; Rodrigues, A. E. *Microporous Mesoporous Mater.* **2011**, *139*, 67−73.

(7) Alaerts, L.; Kirschhock, C. E. A.; Maes, M.; van der Veen, M. A.; Finsy, V.; Depla, A.; Martens, J. A.; Baron, G. V.; Jacobs, P. A.; Denayer, J. E. M.; De Vos, D. E. *Angew. Chem., Int. Ed.* **2007**, *46*, 4293−4297.

(8) Alaerts, L.; Maes, M.; Giebeler, L.; Jacobs, P. A.; Martens, J. A.; Denayer, J. F. M.; Kirschhock, C. E. A.; De Vos, D. E. *J. Am. Chem. Soc.* **2008**, *130*, 14170−14178.

(9) Finsy, V.; Verelst, H.; Alaerts, L.; De Vos, D.; Jacobs, P. A.; Baron, G. V.; Denayer, J. F. M. *J. Am. Chem. Soc.* **2008**, *130*, 7110−7118.

(10) Alaerts, L.; Maes, M.; Jacobs, P. A.; Denayer, J. F. M.; De Vos, D. E. *Phys. Chem. Chem. Phys.* **2008**, *10*, 2979−2985.

(11) Finsy, V.; Kirschhock, C. E. A.; Vedts, G.; Maes, M.; Alaerts, L.; De Vos, D. E.; Baron, G. V.; Denayer, J. F. M. *Chem.—Eur. J.* **2009**, *15*, 7724−7731.

(12) Alaerts, L.; Maes, M.; van der Veen, M. A.; Jacobs, P. A.; De Vos, D. E. *Phys. Chem. Chem. Phys.* **2009**, *11*, 2903−2911.

(13) Maes, M.; Vermoortele, F.; Alaerts, L.; Couck, S.; Kirschhock, C. E. A.; Denayer, J. F. M.; De Vos, D. E. *J. Am. Chem. Soc.* **2010**, *132*, 15277−15285.

(14) Maes, M.; Vermoortele, F.; Alaerts, L.; Denayer, J. F. M.; De Vos, D. E. *J. Phys. Chem. C* **2011**, *115*, 1051−1055.

(15) Nicolau, M. P. M; Barcia, P. S.; Gallegos, J. M.; Silva, J. A. C.; Rodrigues, A. E.; Chen, B. L. *J. Phys. Chem. C* **2009**, *113*, 13173−13179.

(16) Moreira, M. A.; Santos, J. C.; Ferreira, A. F. P.; Loureiro, J. M.; Rodrigues, A. E. *Ind. Eng. Chem. Res.* **2011**, *50*, 7688−7695.

(17) Gu, Z. Y.; Jiang, D. Q.; Wang, H. F.; Cui, X. Y.; Yan, X. P. *J. Phys. Chem. C* **2009**, *114*, 311−316.

(18) Gu, Z. Y.; Yan, X. P. *Angew. Chem., Int. Ed.* **2010**, *49*, 1477−1480.

(19) Jin, Z.; Zhao, H. Y.; Zhao, X. J.; Fang, Q. R.; Long, J. R.; Zhu, G. S. *Chem. Commun.* **2010**, *46*, 8612−8614.

(20) Hartmann, M.; Kunz, S.; Himsl, D.; Tangermann, O.; Ernst, S.; Wagener, A. *Langmuir* **2008**, *24*, 8634−8642.

(21) Lamia, N.; Jorge, M.; Granato, M. A.; Meida Paz, F. A.; Chevreau, H.; Rodrigues, A. E. *Chem. Eng. Sci.* **2009**, *64*, 3246−3259.

(22) Ferreira, A. F. P.; Santos, J. C.; Plaza, M. G.; Lamia, N.; Loureiro, J. M.; Rodrigues, A. E. *Chem. Eng. J.* **2011**, *167*, 1−12.

(23) Li, K.; Olson, D. H.; Seidel, J.; Emge, T. J.; Gong, H.; Zeng, H.; Li, J. *J. Am. Chem. Soc.* **2009**, *131*, 10368−10369.

(24) Gucuyener, C.; van den Bergh, J.; Gascon, J.; Kapteijn, F. *J. Am. Chem. Soc.* **2010**, *132*, 17704−17706.

(25) Cychosz, K. A.; Wong-Foy, A. G.; Matzger, A. J. *J. Am. Chem. Soc.* **2008**, *130*, 6938.

(26) Cychosz, K. A.; Wong-Foy, A. G.; Matzger, A. J. *J. Am. Chem. Soc.* **2009**, *131*, 14538−14543.

(27) Achmann, S.; Hagen, G.; Hämmerle, M.; Malkowsky, I. M.; Kiener, C.; Moos, R. *Chem. Eng. Technol.* **2010**, *33*, 275−280.

(28) Cychosz, K. A.; Matzger, A. J. *Langmuir* **2010**, *26*, 17198−17202.

(29) Serre, C.; Bourrelly, S.; Vimont, A.; Ramsahye, N. A.; Maurin, G.; Llewellyn, P. L.; Daturi, M.; Filinchuk, Y.; Leynaud, O.; Barnes, P.; Ferey, G. *Adv. Mater.* **2007**, *19*, 2246.

(30) Finsy, V.; Kirschhock, C. E. A.; Vedts, G.; Maes, M.; Alaerts, L.; De Vos, D. E.; Baron, G. V.; Denayer, J. F. M. *Chem.—Eur. J.* **2009**, *15*, 7724−7731.

(31) Moggach, S.; Bennett, T.; Cheetham, A. *Angew. Chem., Int. Ed.* **2009**, *121*, 7221−7223.

(32) Fairen-Jimenez, D.; Moggach, S. A.; Wharmby, M. T.; Wright, P. A.; Parsons, S.; Duren, T. *J. Am. Chem. Soc.* **2011**, *133*, 8900−8902.

(33) van Well, W. J. M.; Wolthuizen, J. P.; Smit, B.; Vanhooff, J. H. C.; Vansanten, R. A. *Angew. Chem., Int. Ed.* **1995**, *34*, 2543−2544.

(34) Vlugt, T. J. H.; Zhu, W.; Kapteijn, F.; Moulijn, J. A.; Smit, B.; Krishna, R. *J. Am. Chem. Soc.* **1998**, *120*, 5599−5600.

(35) Calero, S.; Smit, B.; Krishna, R. *Phys. Chem. Chem. Phys.* **2001**, *3*, 4390−4398.

(36) van Well, W. J. M.; Cottin, X.; de Haan, J. W.; van Santen, R. A.; Smit, B. *Angew. Chem., Int. Ed.* **1998**, *37*, 1081−1083.

(37) Mellot, C.; Simonot-Grange, M. H.; Pilverdier, E.; Bellat, J. P.; Espinat, D. *Langmuir* **1995**, *11*, 1726−1730.

(38) Pichon, C.; Methivier, A.; Simonot-Grange, M. H.; Baerlocher, C. *J. Phys. Chem. B* **1999**, *103*, 10197−10203.

(39) Altshuller, A. P. *J. Phys. Chem.* **1955**, *59*, 32−34.

(40) Altschuller, A. P. *J. Phys. Chem.* **1953**, *57*, 538−540.

(41) Webster, C. E.; Drago, R. S.; Zerner, M. C. *J. Am. Chem. Soc.* **1998**, *120*, 5509.

(42) Bordiga, S.; Regli, L.; Bonino, F.; Groppo, E.; Lamberti, C.; Xiao, B.; Wheatley, P. S.; Morris, R. E.; Zecchina, A. *Phys. Chem. Chem. Phys.* **2007**, *9*, 2676−2685.

(43) Dietzel, P. D. C.; Panella, B.; Hirscher, M.; Blom, R.; Fjellvag, H. *Chem. Commun.* **2006**, 959−961.

(44) Peralta, D.; Chaplais, G.; Simon-Masseron, A. I.; Barthelet, K.; Pirngruber, G. D. *Microporous Mesoporous Mater.* **2012**, *153*, 1−7.

(45) Camblor, M. A.; Corma, A.; Valencia, S. *Chem. Commun.* **1996**, 2365.

(46) Liu, Y. L.; Kravtsov, V. C.; Larsen, R.; Eddaoudi, M. *Chem. Commun.* **2006**, 1488−1490.

(47) Nouar, F.; Eckert, J.; Eubank, J. F.; Forster, P.; Eddaoudi, M. *J. Am. Chem. Soc.* **2009**, *131*, 2864−2870.

(48) Kresse, G.; Joubert, D. *Phys. Rev. B* **1999**, *59*, 1758.

(49) Kresse, G.; Hafner, J. *Phys. Rev. B* **1994**, *49*, 14251.

(50) Perdew, J.; Burke, K.; Ernzerhof, M. *Phys. Rev. Lett.* **1996**, 3865.

(51) Vosko, S. H.; Wilk, L.; Nusair, M. *Can. J. Phys.* **1980**, *58*, 1200.

(52) Grimme, S. *J. Comput. Chem.* **2006**, *27*, 1787.

(53) Chui, S. S. Y.; Lo, S. M. F.; Charmant, J. P. H.; Orpen, A. G.; Williams, I. D. A. *Science* 1999, *283*, 1148−1150.

(54) Liu, J. C.; Culp, J. T.; Natesakhawat, S.; Bockrath, B. C.; Zande, B.; Sankar, S. G.; Garberoglio, G.; Johnson, J. K. *J. Phys. Chem. C* **2007**, *111*, 9305−9313.

(55) Park, K. S.; Ni, Z.; Cote, A. P.; Choi, J. Y.; Huang, R. D.; Uribe-Romo, F. J.; Chae, H. K.; O'Keeffe, M.; Yaghi, O. M. *Proc. Natl. Acad. Sci. U. S. A.* **2006**, *103*, 10186−10191.

(56) Huang, X. C.; Lin, Y. Y.; Zhang, J. P.; Chen, X. M. *Angew. Chem., Int. Ed.* **2006**, *45*, 1557−1559.

(57) Luebbers, M. T.; Wu, T.; Shen, L.; Masel, R. I. *Langmuir* **2010**, *26*, 15625−15633.

(58) Banerjee, R.; Phan, A.; Wang, B.; Knobler, C.; Furukawa, H.; O'Keeffe, M.; Yaghi, O. M. *Science* **2008**, *319*, 939−943.
(59) Cottier, V.; Bellat, J. P.; SimonotGrange, M. H.; Methivier, A. *J. Phys. Chem. B* **1997**, *101*, 4798−4802.
(60) Schenk, M.; Vidal, S. L.; Vlugt, T. J. H.; Smit, B.; Krishna, R. *Langmuir* **2001**, *17*, 1558−1570.
(61) Schenk, M.; Calero, S.; Maesen, T. L. M.; Vlugt, T. J. H.; van Benthem, L. L.; Verbeek, M. G.; Schnell, B.; Smit, B. *J. Catal.* **2003**, *214*, 88−99.
(62) Krishna, R.; Calero, S.; Smit, B. *Chem. Eng. J.* **2002**, *88*, 81−94.
(63) Krishna, R.; Smit, B.; Calero, S. *Chem. Soc. Rev.* **2002**, *31*, 185−194.
(64) Cousin Saint Remi, J.; Remy, T.; Van Hunskerken, V.; van dePerre, S.; Duerinck, T.; Maes, M.; De Vos, D.; Gobechiya, E.; Kirschhock, C. E. A.; Baron, G. V.; Denayer, J. F. M. *ChemSusChem* **2011**, *4*, 1074−1077.
(65) van denBergh, J.; Gucuyener, C.; Pidko, E. A.; Hensen, E. J. M.; Gascon, J.; Kapteijn, F. *Chem.—Eur. J.* **2011**, *17*, 8832−8840.
(66) Aguado, S.; Bergeret, G.; Titus, M. P.; Moizan, V.; Nieto-Draghi, C.; Bats, N.; Farrusseng, D. *New J. Chem.* **2011**, *35*, 546−550.
(67) Reyes, S. C.; Santiesteban, J. G.; Ni, Z.; Paur, C. S.; Kortunov, P.; Zengel, J.; Deckman, H. W. Separation of carbon dioxide from nitrogen utilizing zeolitic imidazolate framework materials. US Pat. Appl. 2009214407A, 2011.
(68) Alexander, B. D.; Dines, T. J. *J. Phys. Chem. A* **2003**, *108*, 146−156.
(69) Poissant, R. R.; Huang, Y. N.; Secco, R. A. *Microporous Mesoporous Mater.* **2004**, *74*, 231−238.
(70) Peralta, D.; Chaplais, G.; Simon-Masseron, A.; Barthelet, K.; Pirngruber, G. D. *Ind. Eng. Chem. Res.* **2012**, DOI: ie202995g.